buildings

MDPI

*Article*

# Efficacy of Fire Protection Techniques on Impact Resistance of Self-Compacting Concrete

**Mervin Ealiyas Mathews [1], Tattukolla Kiran [2], Anand Nammalvar [2,*], A. Diana Andrushia [3] and U. Johnson Alengaram [4,*]**

[1] L&T EduTech, Larsen & Toubro Limited, Chennai 600116, India; mervi.567@gmail.com
[2] Department of Civil Engineering, Karunya Institute of Technology and Sciences, Coimbatore 641114, India
[3] Department of Electronics and Communication Engineering, Karunya Institute of Technology and Sciences, Coimbatore 641114, India; diana@karunya.edu
[4] Centre for Innovative Construction Technology (CICT), Department of Civil Engineering, Faculty of Engineering, University Malaya, Kuala Lumpur 50603, Malaysia
* Correspondence: nanand@karunya.edu (A.N.); johnson@um.edu.my (U.J.A.)

**Abstract:** The present research investigates the behaviour of sustainable Self-Compacting Concrete (SCC) when subjected to high temperatures, focusing on workability, post-fire impact resistance, and the effects of fire protection coatings. To develop environmentally friendly SCC mixes, Supplementary Cementitious Materials (SCM) such as Fly Ash (FA), Ground Granulated Blast Furnace Slag (GGBFS), and Expanded Perlite Aggregate (EPA) were used. Fifty-six cubes and ninety-six impact SCC specimens were cast and cured for testing. Fire-resistant Cement Perlite Plaster (CPP) coatings were applied to the protected specimens, a passive protection coating rarely studied. SCC (unprotected and protected) specimens, i.e., protected and unprotected samples, were heated following the ISO standard fire curve. An extensive comparative study has been conducted on utilising different SCMs for developing SCC. Workability behaviour, post-fire impact resistance, and the influence of fire protection coatings on sustainable SCC subjected to high temperatures are the significant parameters examined in the present research, including physical observations and failure patterns. The test results noted that after 30 min of exposure, the unprotected specimen exhibited a significant decrease in failure impact energy, ranging from 80% to 90%. Furthermore, as the heating duration increased, there was a gradual rise in the loss of failure impact energy. However, when considering the protected CPP specimens, it was observed that they effectively mitigated the loss of strength when subjected to elevated temperature. Therefore, the findings of this research may have practical implications for the construction industry and contribute to the development of sustainable and fire-resistant SCC materials.

**Keywords:** self-compacting concrete; post-fire impact resistance; expanded perlite aggregate; high temperature; impact failure energy



**Citation:** Mathews, M.E.; Kiran, T.; Nammalvar, A.; Andrushia, A.D.; Alengaram, U.J. Efficacy of Fire Protection Techniques on Impact Resistance of Self-Compacting Concrete. *Buildings* **2023**, *13*, 1487. https://doi.org/10.3390/buildings13061487

Academic Editor: Andrea Benedetti

Received: 14 April 2023
Revised: 1 June 2023
Accepted: 7 June 2023
Published: 8 June 2023



## 1. Introduction

Concrete is extensively employed in infrastructure development on a global scale and has a production rate of around 25 billion tonnes per year, as estimated in 2009 [1]. Compaction is a crucial step in traditional concrete casting [2]. It involves placing the mixture in a mould and compressing it using vibrators to eliminate trapped air and compact the ingredients within the mould to attain the required strength, permeability, and durability for the structural system [3]. Inadequate compaction can lead to reduced stability and inferior-quality concrete, while excessive vibration can negatively impact the overall structural integrity [4]. In-depth research on the passive fire protection of concrete structures was carried out by Gabriel Alexander Khoury. Various theories have been put forward to explain the heating rate of concrete at the interface, the analysis of thermal spalling, and the impact of concrete matrix characteristics such as cementitious composite content, initial

moisture content, and aggregate type under elevated temperatures [5]. This approach provides a higher level of scientific accuracy, resulting in more conservative and safer outcomes in relation to fire hazards. Furthermore, it presents advantages in suggesting new design possibilities and promoting the careful and cost-effective application of thermal barriers and fire protection (passive) for concrete [6].

In 1986, a novel form of concrete called self-compacting/consolidating concrete was introduced by Okamura [7]. In contrast to conventional concrete, SCC does not necessitate any vibration or consolidation during the placement process. Due to its inherent weight, SCC effortlessly fills the formwork and smoothly flows around densely arranged reinforcements. SCC is characterised by its remarkable flow properties, such as flowability, passing, and filling ability. The intrinsic fresh characteristics of concrete contribute to the reduction of both construction time and cost. The mixture is enhanced in developing SCC by incorporating SCMs derived from industrial waste products with binder characteristics [8]. The advancement of SCC is motivated by augmenting the fine aggregate and reducing the clinker content. This is achieved using diverse SCMs like FA, GGBFS, Silica, metakaolin, limestone minerals, and other alternatives [9]. This highlights the need for extensive research on SCC development.

To analyse the workability of the SCC mixture, the EFNARC 2005 guidelines recommended assessing its flow rate, filling capacity, passing capabilities, and resistance to segregation [10]. To improve the flow properties and reduce segregation in SCC, the inclusion of a superplasticizer (SP) and a viscosity-modifying agent (VMA) can be considered [11]. To mitigate segregation, adding an appropriate quantity of VMA or increasing powder content can effectively maintain the suspension of aggregates within the binder region without impeding the flow [12].

Throughout the lifespan of a structure, concrete can experience significant deterioration in its physical, mechanical, and durability characteristics due to exposure to different loading events and adverse conditions [13]. Fire is one of the significant threats to structures, and it may severely reduce the strength of concrete elements [14]. Beyond 600 °C, SCC compressive strength decreases significantly [15]. Apart from the decline in compressive strength, the bond strength also experiences degradation beyond a temperature of 700 °C [16]. The chemical breakdown of cement components in high temperatures is the main cause of property deterioration. This includes factors such as thermal incompatibility, loss of bond in the interfacial transition zone (ITZ), disruption of the gel structure of calcium silicate hydrates (CSH), substantial pore water pressure, and the formation of tensile stress [17]. Currently, there is limited available data on the influence of temperature on the strength characteristics of SCC when mineral admixtures are introduced [18].

Impact resistance is paramount when designing airport runways, landing areas, and military facilities in conflict zones. ACI 544-2R has put forward a cost-effective and straightforward mass drop test as a means to assess the residual impact strength of concrete [19]. This test uses a small-scale concrete disk measuring 150 mm in diameter and 63.50 mm in thickness. And it does not require high-end facilities or measuring equipment, making it highly accurate [20]. Previous studies have extensively examined the behaviour of SCC and other high-performance concretes when subjected to high temperatures. According to Table 1 in the database, it has been noted that an increase in temperature exposure leads to a significant decline in the strength properties of concrete [21–26]. Despite this, there is considerably less investigation into the impact resistance of sustainable SCC subjected to elevated temperatures. The present study has conducted detailed research on crack patterns and failure analysis of SCC after prolonged temperature exposure, which was not observed in previous studies [27]. Additionally, the present research focused on the temperature resistance of concrete by using passive protection coatings such as EPA and GPP, which have rarely been studied.

**Table 1.** Experimental database properties from past studies.

| Authors | Type of Concrete (i) | Admixture Type/Other Ingredients (ii) | Temperature (°C) | Mode of Testing | Types of Tests (iii) | Remarks |
|---|---|---|---|---|---|---|
| Al-Ameri et al. [21] | NSC | OPC | 100, 200, 300, 400, 500 and 600 | Residual condition | CS, FS, IS. | The strength of concrete diminishes by 50% when subjected to a temperature of 600 °C compared to the unheated specimen. Additionally, the impact strength of concrete experiences deterioration at 600 °C. |
| Mezzal et al. [22] | HSCC | SF | 300, 500 and 700 | Residual condition | CS, TS, FS, and IS. | At higher temperatures, the HSCC specimens show a higher impact resistance value than SCC. |
| Abid et al. [20] | SFRC | SF | 200, 400 and 600 | Residual condition | WL, CS, and IS. | The specimens lost the impact resistance after exposure to 400 °C and 600 °C. |
| Khaliq and Kodur [23] | SCC | SF, PF, and HF. | 20, 200, 400, 600 and 800 | Un-stressed condition | CS, TS, and ME | At 400 °C, the SCC-SF, SCC-PF, and SCC-HF showed no strength loss than the reference specimen. |
| Rios et al. [24] | HSSC | PF | 20, 100, 300, 500 and 700 | Un-stressed and residual condition | CS, TS, and ME | With the addition of fibers, the spalling and voids of concrete reduce significantly. |
| Aslani et al. [14] | HSPFC | PF | 20, 200, 400, 600, 800 and 900 | Residual condition | CS, TS, and ME | With the addition of PF, concrete spalling and shrinkage cracks decrease significantly. |
| Eidan et al. [26] | FRC | PF | 20, 100, 200, 300, 400, 500 and 600 | Residual condition | CS, TS, and ME | PF shows less spalling and cracks in concrete after elevated temperature. |

Abbreviations: (i) FRC: Fibre Reinforced Concrete, HSSCC: High Strength Self-Compacting Concrete, HSPFC: High Strength Polypropylene Fibre Reinforced Concrete, NSC: Normal Strength Concrete; (ii) FRC: Fibre Reinforced Concrete; SF: Steel Fibre, PF: Polypropylene Fibre, HF: Hybrid Fibre, and OPC: Ordinary Portland Cement; (iii) CS: Compressive Strength, TS: Tensile Strength, FS: Flexural Strength, ME: Modulus of Elasticity, and WL: Weight Loss.

The purpose of this research is to evaluate SCC's impact resistance during high-temperature exposure. The study will investigate how SCMs affect SCC performance over different temperature ranges. Additionally, the study aims to improve the residual impact load capacity of SCC following high-temperature exposure and analyse the behaviour of CPP post-temperature exposure.

## 2. Experimental Investigation

### *2.1. Materials*

This section provides a comprehensive account of the materials employed in the study, encompassing their physical and chemical properties, mix design, and the methodology adopted for specimen preparation.

#### 2.1.1. Supplementary Cementitious Materials

In this study, concrete samples were prepared using Ordinary Portland Cement (OPC) of 53-grade that complied with the specifications outlined in IS 12269 (2013) [28]. For this investigation, the study incorporated Class-F FA and GGBFS as SCMs. Class-F FA exhibits pozzolanic reactivity with the lime generated during cement hydration. Additionally, GGBFS, a by-product of the steel industry, was employed in the study.

Expanded perlite aggregate (EPA) is a lightweight and porous material derived from siliceous volcanic rock. It can remarkably expand up to twenty times its original volume and features a white appearance. EPA possesses several advantageous physical properties, such as reduced mass density, limited thermal conduction, and excellent heat resistance,

making it suitable for various commercial applications. An overview of the chemical and physical characteristics of the SCMs and EPAs is presented in Table 2.

**Table 2.** Chemical and physical characteristics of SCM and EPA.

| Oxides | Chemical Properties (%) | | | |
|---|---|---|---|---|
| | **OPC** | **FA** | **GGBFS** | **EPA** |
| $SiO_2$ | 20.12 | 60.20 | 38.72 | 73.50 |
| $Fe_2O_3$ | 3.41 | 3.42 | 1.12 | 1.21 |
| $Al_2O_3$ | 8.53 | 28.24 | 14.43 | 7.56 |
| CaO | 61.31 | 4.96 | 37.35 | 0.92 |
| MgO | 2.26 | 0.31 | 8.12 | 1.12 |
| $Na_2O$ | 1.81 | 0.55 | 0.17 | 2.86 |
| $K_2O$ | 2.71 | 1.27 | 0.92 | 5.6 |
| $SO_3$ | 0.24 | 2.25 | 0.26 | 6.2 |
| Loss on ignition | 0.05 | 0.09 | 0.01 | 0.025 |
| **Properties** | **Physical Properties** | | | |
| | **OPC** | **FA** | **GGBFS** | **EPA** |
| Specific gravity | 3.15 | 2.38 | 2.45 | 2.12 |
| Density ($kg/m^3$) | 3200 | 1580 | 1786 | 675 |
| Surface area ($m^2/kg$) | 3310 | 892 | 1200 | - |
| Colour | Pale grey | Light grey | Whitish | White |

### 2.1.2. Filler Materials

The experimental study employed Manufactured Sand (M-Sand or MS), finely crushed material smaller than 4.76 mm in size, meeting the specifications of the Zone II category. According to the "The "IS 383:2016—Specifications for Fine and Coarse Aggregate from Natural Sources for Concrete of the Indian Standard code of practice, Zone II sand is expected to possess a fineness modulus ranging between 2.2 and 2.6, as well as a specific gravity falling within the range of 2.5 to 2.9. Concrete mixtures with compressive strengths up to 50 MPa are deemed appropriate for using Zone II sand. The physical characteristics of MS were determined following IS 383 (2016) [29]. Coarse aggregates (CA) in this study consisted of crushed stones with a size of 12 mm and below. To partially replace MS, an optimal amount of EPA was added, equivalent to 2.5% of the MS content. The properties of the aggregates can be found in Table 3, while Figure 1 depicts the particle size distribution of both MS and CA. To ensure the desired flow characteristics of fresh concrete while minimizing the powder content, a polycarboxylate ether-based SP was employed. Additionally, a VMA was incorporated to prevent particle segregation.

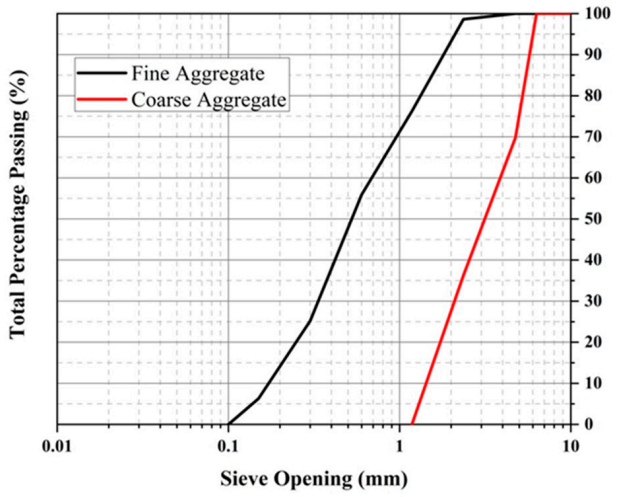


**Figure 1.** Granulometric curve of MS and CA.

**Table 3.** Physical properties of MS and CA.

| Aggregate Type | Density (kg/m$^3$) | Specific Gravity | Water Absorption (%) |
|---|---|---|---|
| MS | 1624 | 2.73 | 0.59 |
| CA | 1792 | 2.82 | 0.46 |

### *2.2. Mix Design and Preparation of Specimens*

In this investigational study, the focus was on developing SCC with five different mix proportions. The workability characteristics of the trial mixes were adjusted in accordance with grading guidelines to meet the specified criteria. The reference mixes were formulated with a fixed composition consisting of 59% OPC, 31% FA or GGBFS, and 0% EPA, based on the findings of the trial mixes. To comply with EFNARC directives, the mixtures of FA and GGBFS in the control mixes were adjusted to the same level as in the trial mixes. The control mix designation depended on the SCM used, with FA referring to Fly Ash and GGBFS indicating Ground Granulated Blast Furnace Slag. In the second phase, the influence of EPA was examined by incorporating it into the mix and replacing 2.5% of the fine aggregate in the control mixes. The final mixes, FA/EPA and GGBFS/EPA were prepared using 59% OPC, 31% FA or GGBFS, and 2.5% MS, which EPA replaced through volume batching. The mix designations followed a naming convention where FA and GGBFS denoted Fly Ash and Ground Granulated Blast Furnace Slag, respectively, and the numerical value followed by EPA represented the percentage of expanded perlite aggregate used as an alternative for the fine aggregate.

Each mix was designed to have a powder content (total cementitious material) of 464 kg/m$^3$ and a CA content of 804 kg/m$^3$. The water-powder ratio was maintained at 0.42, with a consistent 218 kg/m$^3$ water content across all mix combinations. The specific mix proportions can be found in Table 4. The CA, MS, and EPA were mixed thoroughly for one minute, after which the binder materials were added to an electric laboratory concrete mixing machine. The dry components were blended for approximately 2 min to achieve a uniform mixture. Subsequently, 70% of the water, along with the superplasticizer (SP), was added gradually to the mixture, followed by a 2-min mixing and 2-min resting period. The remaining water was then introduced, and the mixer drum was rotated for an additional 3 min to complete the mixing process. The freshly prepared SCC mixture was carefully poured into a steel mould to assess its performance under load. To prevent water evaporation and facilitate the setting process, the mould containing the concrete was securely covered with polythene sheets for 24 h. After the specified period, the specimens were demoulded and transferred to a curing tank to initiate the hydration reaction. The samples were allowed to undergo the curing process in the tank for 28 days.

**Table 4.** SCC mix proportions.

| Mix | Mix Proportions (kg/m$^3$) | | | | | | | | | |
|---|---|---|---|---|---|---|---|---|---|---|
| | OPC | w/p | SP | VMA | Water | FA | GGBFS | EPA | Aggregates | |
| | | | | | | | | | CA | MS |
| FA | 320 | 0.42 | 0.8 | 0.10 | 218 | 144 | - | - | 804 | 963 |
| FA/EPA | 320 | 0.42 | 0.9 | 0.15 | 218 | 144 | - | 24 | 804 | 939 |
| GGBFS | 320 | 0.42 | 0.9 | 0.15 | 218 | - | 144 | - | 804 | 963 |
| GGBFS/EPA | 320 | 0.42 | 1.0 | 0.20 | 218 | - | 144 | 24 | 804 | 939 |

Note: w/p = water–powder ratio.

### *2.3. Test Procedure*

The details of the fresh properties of SCC are elaborated below.

SCC Rheological Properties

The facility of SCC to effectively fill densely packed formwork and prevent segregation was assessed using a range of test methods in accordance with the EFNARC guidelines. The filling capacity was evaluated through tests such as slump flow and $T_{500}$. The flowability and consistency of the concrete were assessed through the J-ring and V-funnel tests to evaluate its passing ability and viscosity. Figure 2 provides a detailed presentation of the workability tests conducted on the SCC. Results obtained from the workability tests conducted is detailed in Table 5.

**Figure 2.** View of workability tests of fresh SCC.

**Table 5.** Test Results of Fresh SCC.

| Tests | Test Results | | | | | |
|---|---|---|---|---|---|---|
| | Mix 1 | Mix 2 | Mix 3 | Mix 4 | EFNARC Criteria | |
| | | | | | Min | Max |
| Slump Flow (mm) | 660 | 665 | 675 | 680 | 640 | 800 (SF 2) |
| $T_{500}$Flow Time (s) | 2.90 | 2.73 | 2.45 | 2.20 | >2 (VF 2) | |
| J-Ring (mm) | 7.00 | 6.60 | 6.20 | 6.00 | 0 | 10 |
| V-Funnel (s) | 10.80 | 10.40 | 11.70 | 11.30 | ≥7 to ≤ 27 (VF 2) | |

*2.4. Development of Protective Coating*

The specimens incorporating a CPP layer were created by applying a plaster made of OPC and EPA mortar (1:4). Through several experiments, a w/c ratio of 0.65 was deemed suitable, and a consistent coating thickness of 20 mm was maintained across all specimens. The physical and strength characteristics of the CPP mortar were then investigated. A fresh CPP mixture was prepared and cast into cubical-shaped specimens measuring 70.6 mm × 70.6 mm × 70.6 mm. The density of the CPP material was found to be 1522 kg/m$^3$, with a water absorption rate of 21.3% and a compressive strength of 19.2 MPa.

*2.5. Elevated Temperature Test*

Before the initiation of heating, both the exposed and protected specimens were dried for one day. A computerized heating furnace, measuring 700 mm × 500 mm and designed to ensure uniform heating of the specimens, was utilized in this study. The heating rate adhered to the standard fire curve. The specimens were heated for 30, 60, 90, and 120 min. Upon reaching the target temperature, the furnace automatically shut off, and the specimens were left to cool down until they reached room temperature naturally. The heating process and the representation of the test specimens are depicted in Figure 3a. After reaching room temperature, the concrete specimens' surface cracks and mass loss were recorded. In contrast, the furnace's temperature profile and the concrete's surface temperature are graphically presented in Figure 3b.

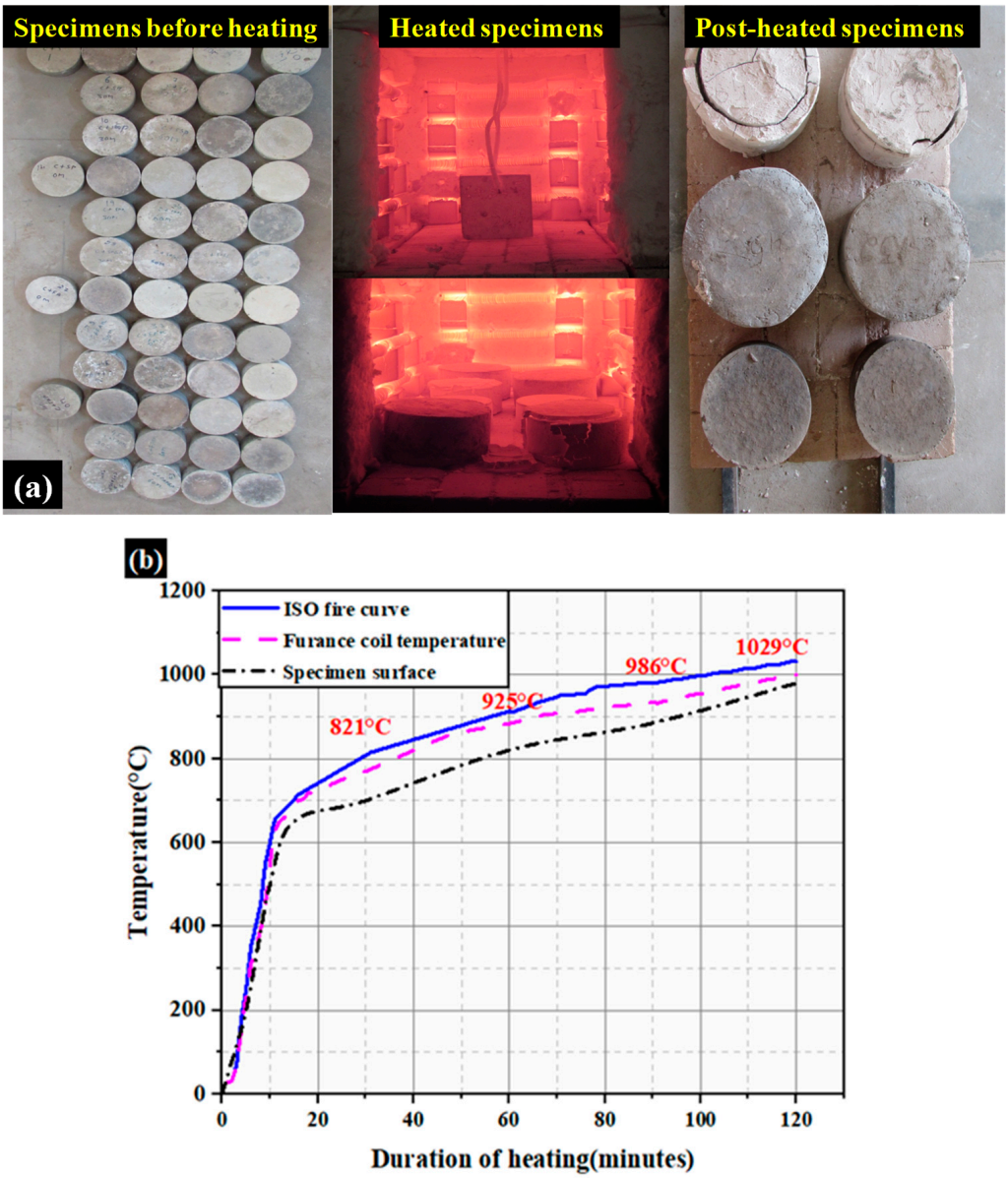


**Figure 3.** (**a**) View of the unheated specimens and heated specimens. (**b**) Time-temperature curve.

### *2.6. Experimental Tests of SCC*

SCC's detailed experimental test procedures (compressive strength, impact strength) are presented below.

#### 2.6.1. Compressive Strength (CS) of SCC

CS, which holds significant importance in structural design, is a critical concrete parameter. Test specimens measuring 150 mm × 150 mm × 150 mm were fabricated specifically for the CS test. The test was carried out utilizing a Compression Testing Machine (CTM) following the prescribed curing process, with a load rate of 14 MPa/minute following the guidelines outlined in IS 516 (2004) [30]. The outcomes of the compressive test on the concrete are illustrated in Figure 4.

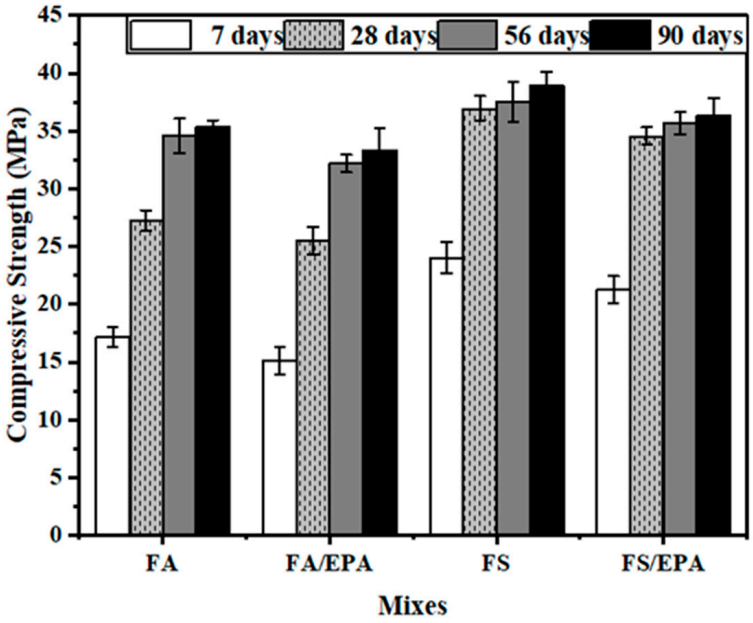


**Figure 4.** Compressive test results of SCC mixes.

The compressive strength of the reference mix, which did not include EPA as a fine aggregate, was higher than the mix containing 2.5% EPA. The decrease in strength can be attributed to several factors, including the inadequate bond between the lightweight mineral aggregate (EPA) and the cement paste. This insufficient bond is mainly influenced by the shape and size of the aggregate, which creates a weak interfacial transition zone (ITZ). Moreover, the presence of EPA in the mixture may also impact the overall consistency of the concrete. Furthermore, including mineral and chemical admixtures in the mix can prolong the initial strength development by delaying the hydration process of cement.

The SCC mix incorporating GGBFS demonstrates a faster rate of strength development and achieves higher strength values due to the hydraulic cementitious properties of the mineral pozzolan. However, varying SP content decreases workability and strength parameters by reducing the demand for high water content. The SCC mix with GGBFS shows the highest strength, with approximately 24.03 MPa at seven days and 38.89 MPa at 90 days. The SCC mix containing GGBFS and 2.5% EPA exhibits a slight reduction in strength, about 11.53% lower than the mix without EPA. Similarly, the reference SCC mix with FA shows similar strength gains as the GGBFS-based mix, measuring approximately 17.15 MPa at seven days and 35.36 MPa at 90 days. Therefore, the GGBFS-based SCC mix demonstrates superior early-age strength development compared to the FA-based SCC mix.

#### 2.6.2. Impact Strength of SCC

For surface crack assessments and impact strength tests, cylindrical SCC samples with a diameter of 150 mm and a height of 63.50 mm were utilized in this study. The cylindrical shape was chosen because it ensures uniform heating during different heating cycles, and any surface cracks that develop on the exposed face are expected to be evenly distributed across the cross-section. The drop weight test method and device depicted in Figure 5 were employed in accordance with the guidelines provided by ACI 544 [31]. To apply the impact load to the specimen, a 45-N hammer was dropped repeatedly from a height of 457 mm onto a hardened steel ball with a diameter of 64 mm. This process was repeated until the specimen failed. The number of blows required for the initial failure and final failure of each specimen was recorded. The initial failure was determined when the first hairline crack appeared on the specimen's surface, while the ultimate failure was observed when the specimen was completely split into multiple parts.

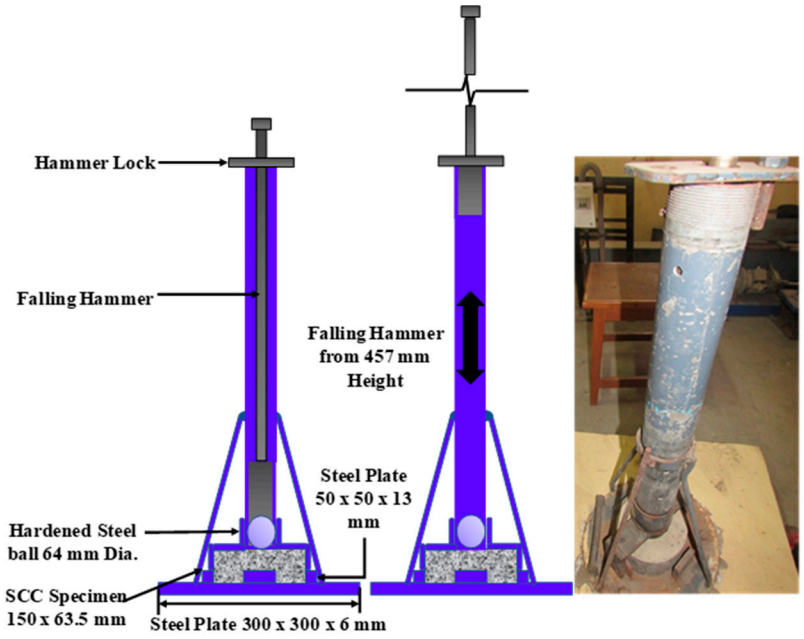


**Figure 5.** Schematic representation and view of impact strength test setup.

## 3. Results and Discussion

### *3.1. Residual Compressive Strength and Mass Loss of SCC after Exposure*

#### 3.1.1. Residual Compressive Strength

Figure 6 presents a graphical representation of the residual compressive strength and mass loss observed in different SCC specimens exposed to varying durations of heating. The residual compressive strength of SCC cube specimens can be classified into distinct phases based on the duration of exposure and their corresponding strength levels. Unprotected specimens of FA and GGBFS without CPP (FA/EPA, FA, GGBFS/EPA & GGBFS) exhibit two phases: 0 to 30 min and 30 to 120 min. Conversely, CPP specimens of FA and GGBFS (FA/EPA/CPP, FA/CPP, GGBFS/EPA/CPP & GGBFS/CPP) display three phases: 0 to 30 min, 30 to 60 min, and 60 to 120 min. Notable differences in residual strength between the two phases of FA and GGBFS specimens without CPP protection are evident. The initial phase (0 to 30 min) exhibits a substantial strength gain, followed by a sharp decline in the second phase (30 to 120 min). The strength gains during the first phase (0 to 30 min) of unprotected specimens (FA/EPA, FA, GGBFS/EPA & GGBFS) range from 12% to 26%. This increase in strength can be attributed to secondary hydration resulting from the autoclave effect on unhydrated clinker [32].

As the duration of temperature exposure extends beyond 30 to 120 min, the decline in strength becomes increasingly pronounced. The most substantial reduction in strength is observed at 60 min (925 °C), with a maximum decay of 16%. Furthermore, unprotected specimens (FA/EPA, FA, GGBFS/EPA & GGBFS) experience a higher loss of approximately 63% at 120 min (1029 °C).

The deterioration of the dense structure and the decline in strength in SCC become significant when exposed to temperatures above 500 °C, primarily due to the decomposition of calcium hydroxide. During this phase, the strength reduction occurs due to the complete dehydration of the CSH gel, resulting in the loss of its inherent binding ability [33].

The protected specimens of FA and GGBFS (FA/EPA/CPP, FA/CPP, GGBFS/EPA/CPP & GGBFS/CPP) display distinct variations in strength patterns based on the duration of exposure. In the initial phase (0 to 30 min), all specimens exhibit a minimal reduction of less than 1% in strength. From 30 to 60 min, a gradual strength gain ranging from 16% to 30% is observed following the initial decline. The CPP-coated FA and GGBFS specimens demonstrate improved performance compared to the unprotected specimens at higher

temperature exposure. Even after 90 min of temperature exposure, the CPP specimens of FA and GGBFS exhibit a strength gain of 12% and 2%, respectively. This enhancement can be attributed to the thermal insulating capability of the perlite mineral, which limits the heat flux into the concrete core, thereby enhancing the performance of the protected specimens [34].

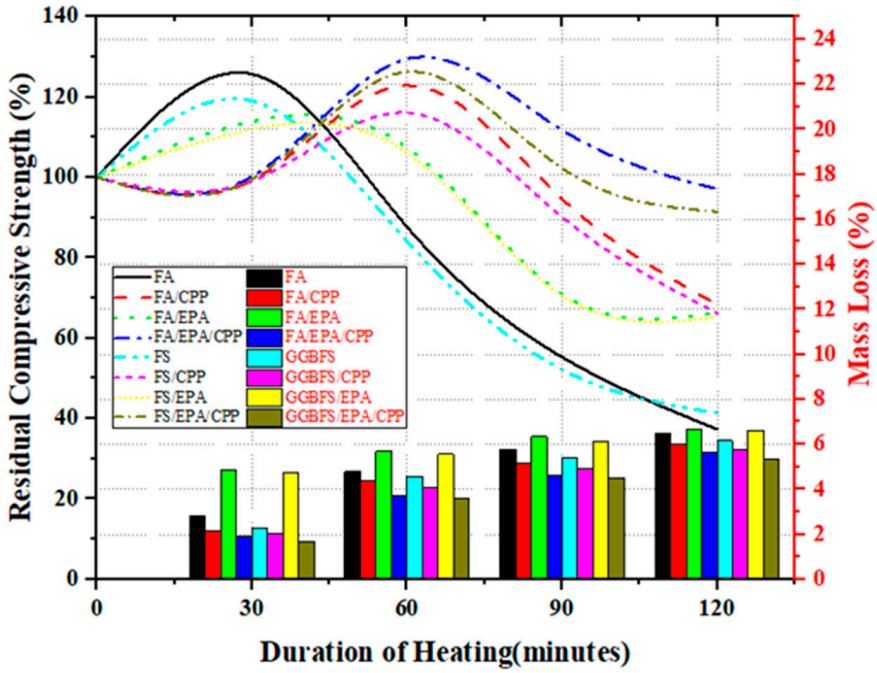


**Figure 6.** Interaction graph showing variation between residual compressive strength (represented by the line) and mass loss (represented by histograms) of SCC specimens for different duration of heating.

In the final phase of temperature exposure (60 to 120 min), a gradual decrease in strength is observed for FA and GGBFS specimens, with a strength loss ranging from 10% to 5%, even lower than that of the unprotected specimens. Based on the results of residual compressive strength, it can be concluded that the perlite mineral can be effectively utilized as a sacrificial coating (CPP layer) on the surface of SCC and as an internal thermal-resistant filler. At 120 min of temperature exposure, the maximum reduction in strength is observed, ranging from 32% to 34% for FA/CPP and GGBFS/CPP specimens, respectively. The observed strength loss for FA/EPA/CPP and GGBFS/EPA/CPP specimens is minimal, with values of 3% and 10%, respectively [14–16].

### 3.1.2. Mass Loss

The initial reduction in mass observed in SCC can be attributed to the evaporation of free and physically bound water, which converts into vapor under high-temperature conditions [35]. This phenomenon typically occurs during the rapid heating phase, which spans up to 60 min of temperature exposure. A comparison of mass loss between specimens of FA and GGBFS without CPP (FA/EPA, FA, GGBFS/EPA & GGBFS) and CPP-coated FA and GGBFS (FA/EPA/CPP, FA/CPP, GGBFS/EPA/CPP & GGBFS/CPP) reveals a range of 5.70% to 4.60% and 3.70% to 4.10%, respectively. The minimal variation in mass loss observed among the SCC specimens can be attributed to the influence of internal EPA content. As the level and duration of temperature increase beyond 60 to 120 min, there is a proportional escalation in mass loss, likely due to the degradation of the gel structure (CSH) and portlandite (CH), leading to a more significant loss in strength [36].

### *3.2. Impact Resistance of SCC after Exposure*

Figure 7a,b presents the impact energy failure and the corresponding number of blows for the SCC specimens (FA, GGBFS, FA/EPA, and GGBFS/EPA) subjected to elevated temperatures. Compared to the heated specimens, the SCC specimens not exposed to heat, including FA, GGBFS, FA/EPA, and GGBFS/EPA, demonstrated higher impact energy levels. The impact energy for the unheated specimens was 913.9 J, 2234.0 J, 812.4 J, and 2132.4 J, respectively. At 30 min of heating duration (821 °C), the failure impact energy was 182.8 J and 223.4 J for the FA 30M (no. of blows: 9) and GGBFS 30M specimens (no. of blows: 11), respectively. SCC specimens with EPA content showed increased failure impact energy value, with the FA/EPA 30M and GGBFS/EPA 30M specimens recording 243.7 J (no. of blows: 12) and 284.3 J (no. of blows: 14), respectively. A decrease in failure impact energy was observed as the heating duration reached 60 min (925 °C), with the FA 60M and GGBFS 60M specimens having failure impact energy values of 121.9 J (no. of blows: 6) and 182.8 J (no. of blows: 9), respectively.

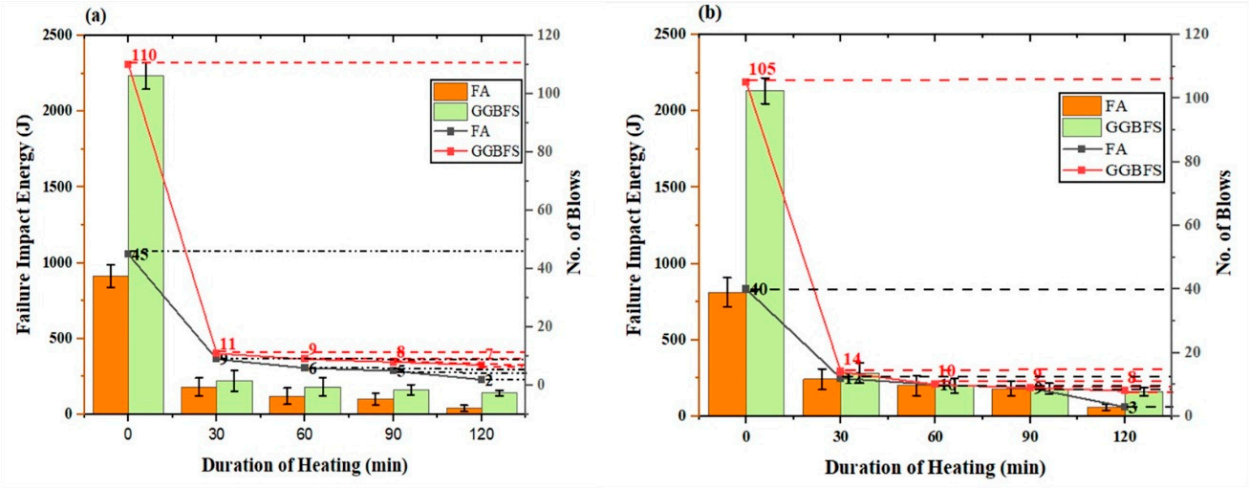


**Figure 7.** Failure impact energy (represented by histograms) and the number of blows of unprotected SSCC specimens subjected to high temperature (represented by the line), (**a**) FA and GGBFS, (**b**) FA/EPA and GGBFS/EPA.

The FA/EPA 60M and GGBFS/EPA 60M SCC specimens exhibited a similar fractional impact energy failure, measured at 203.1 J (number of blows: 10). After 90 min of heating (986 °C), the failure impact energy decreased to 101.5 J (number of blows: 5) for the FA 90M specimen and increased to 3162.5 J (number of blows: 8) for the GGBFS 90M specimen. The FA/EPA 90M and GGBFS/EPA 90M specimens demonstrated a failure impact energy of 182.8 J. The inclusion of the EPA showed a crucial role in mitigating the reduction in impact energy caused by temperature exposure exceeding 30 min. Further increasing the duration to 120 min (1029 °C) led to a notable decrease in failure impact energy to 40.6 J, 142.2 J, 60.9 J, and 162.5 J for the FA, GGBFS, FA/EPA, and GGBFS/EPA specimens, respectively. SCC mixes incorporating GGBFS (GGBFS 0M and GGBFS/EPA 0M) exhibited delayed setting times but enhanced impact resistance. The overall raise in strength can be attained by the latent hydraulic properties of the material, which reacted with the ($Ca(OH_2)$) formed during the hydration process [37].

### *3.3. Failure Impact Energy of SCC Specimens*

Figure 8a,b depict the variations in failure impact energy and the corresponding number of blows for the unprotected (FA and GGBFS) and protected SCC specimens subjected to high temperatures. The results of impact energy failure revealed that the specimens with CPP coating containing EPA demonstrated superior performance under impact loading conditions. This can be attributed to the enhanced thermal compatibility of

the CPP layers, which effectively limited the transfer of heat transfer into the core of the SCC, resulting in reduced impact energy. Generally, the failure energy decreased as the intensity of exposure and the duration of heating increased. The graphical examination indicated that the SCC specimens incorporating EPA and protected by a CPP layer, FA/EPA/CPP and GGBFS/EPA/CPP, exhibited superior performance across all exposure conditions.

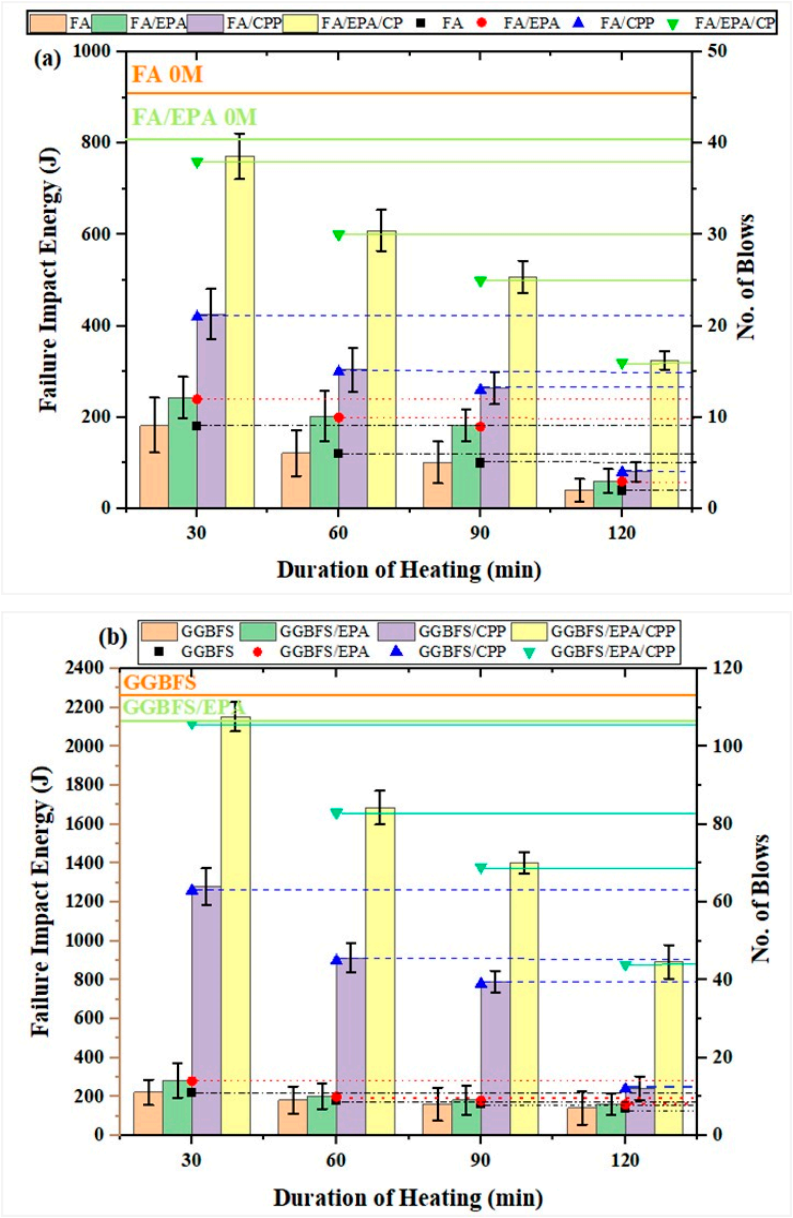


**Figure 8.** (**a**) Failure impact energy (represented by histograms) and the corresponding number of blows of protected SCC (FA) specimens exposed to elevated temperature (represented by the dots). (**b**) Failure impact energy (represented by histograms) and the corresponding number of blows of protected SCC (GGBFS) specimens exposed to elevated temperature (represented by the dots).

The FA/EPA/CPP 30M specimen exhibited a loss in failure impact energy of about 15.56%, while it was 80% for unprotected FA 30M specimens. The difference in the failure impact energy loss of GGBFS/EPA/CPP 30M and GGBFS 30M compared to that of the GGBFS 0M specimen was about 3.6% and 90%, respectively. The efficiency of the CPP coating in combination with the EPA content in withstanding high temperatures is evident

from the comparison. EPA's enhanced thermal compatibility nature gives it a unique property [32,33].

The heated specimens FA/EPA/CPP 60M and GGBFS/EPA/CPP 60M exhibited impact energy losses of 33.3% and 24.6%, respectively, compared to the FA 0M and GGBFS 0M specimens. On the other hand, the unprotected heated specimens FA 60M and GGBFS 60M demonstrated significantly higher impact energy losses of approximately 86.7% and 91.8%, respectively, when compared to the FA 0M and GGBFS 0M specimens. The failure impacts energy values of SCC-FA and SCC-GGBFS specimens are presented in Tables 6 and 7, respectively.

**Table 6.** View of failure impacts energy values (in J) of SCC-FA and coated (EPA/CPP) specimens.

| Duration of Heating (min) | Specimen Type | | | |
|---|---|---|---|---|
| | FA | FA/EPA | FA/CPP | FA/EPA/CPP |
| 30 | 182.7 | 243.7 | 426.4 | 771.7 |
| 60 | 121.8 | 203.1 | 304.6 | 609.2 |
| 90 | 101.5 | 182.7 | 264.1 | 507.7 |
| 120 | 40.6 | 60.9 | 81.2 | 324.9 |

**Table 7.** View of failure impacts energy values (in J) of SCC-GGBFS and coated (EPA/CPP) specimens.

| Duration of Heating (min) | Specimen Type | | | |
|---|---|---|---|---|
| | GGBFS | GGBFS/EPA | GGBFS/CPP | GGBFS/EPA/CPP |
| 30 | 223.3 | 284.3 | 1279.4 | 2152.7 |
| 60 | 182.7 | 203.1 | 913.8 | 1685.6 |
| 90 | 162.4 | 182.7 | 792.1 | 1401.3 |
| 120 | 142.1 | 162.4 | 243.7 | 893.5 |

The loss in failure impact energy for the FA/EPA/CPP 120M specimen was approximately 44.44%, whereas the unprotected FA 90M specimens showed a loss of 88.9%. The reduction in failure impact energy for GGBFS/EPA/CPP 30M and GGBFS 30M specimens compared to the GGBFS 0M specimen was approximately 37.3% and 92.7%, respectively.

All test specimens experienced a rapid decline in failure impact energy when temperature exposure exceeded 120 min. However, the protected specimens could limit energy loss compared to the unprotected ones [38]. The loss in impact energy for 120 min of heated FA/EPA/CPP and GGBFS/EPA/CPP was 64.4% and 60.0%, respectively, compared to FA 0M and GGBFS 0M specimens. Unprotected heated specimens (FA 120M and GGBFS 120M) showed a significantly more significant loss in impact energy of around 95.6% and 93.6%, respectively, compared to FA 0M and GGBFS 0M specimens. The study found that even after 120 min of heating, the CPP-protected SCC specimens containing EPA effectively resisted temperature penetration and reduced the loss in failure impact energy [39].

During the heating period, measurements were taken to determine the time-temperature behaviour of various specimens, including FA, FA/EPA, FA/CPP, FA/EPA/CPP, GGBFS, GGBFS/EPA, GGBFS/CPP, and GGBFS/EPA/CPP. Temperatures were recorded at each specimen's surface, protective layer, and core. For FA/EPA specimens exposed to 60 min of heating, the measured temperatures were 918 °C at the concrete surface and 613 °C at the core. After 90 min of exposure, the surface temperature reached 922 °C, while the core temperature rose to 756 °C. At the end of the 120-min exposure, the surface temperature measured 1012 °C, and the core temperature was 883 °C. Similarly, for GGBFS/EPA specimens exposed to 60 min of heating, the recorded surface temperature was slightly higher at 920 °C than the FA/EPA specimen (637 °C). A similar temperature increase pattern was observed after 120 min of heating, with surface temperatures of 1025 °C and 899 °C and core temperatures of 1025 °C and 899 °C for GGBFS/EPA and FA/EPA specimens, respectively.

For specimens protected by the CPP layer, the surface, protective layer, and core temperatures at 60 min of heating were 918 °C, 492 °C, and 205 °C, respectively, for FA/EPA/CPP specimens and 920 °C, 463 °C, and 159 °C, respectively, for GGBFS/EPA/CPP specimens. A similar pattern was observed for the 90-min exposure duration. At 120 min of heating, the temperatures measured for FA/EPA/CPP specimens were 979 °C, 892 °C, and 605 °C for the surface, protective layer, and core, respectively, while the corresponding temperatures for GGBFS/EPA/CPP specimens were 981 °C, 871 °C, and 556 °C. The measurements indicate that as time and temperature increased, the penetration of temperature into the concrete specimens also increased.

### *3.4. SCC Crack Analysis of SCC Specimens Subjected to High Temperature*

When concrete structures are subjected to elevated temperatures, there is a risk of thermal crack formation. The combination of high heat flux on the concrete surface, coupled with the thermal incompatibility between the mortar and aggregate, contributes to the formation of microcracks. To effectively manage these cracks, it is crucial to precisely measure their geometrical characteristics, including width, length, density, and pattern [40]. This study aims to analyse the crack pattern in SCC and explore potential strategies to control these cracks under standard fire temperature conditions.

Figure 9a, b illustrates the failure patterns of SCC specimens, protected (FA/EPA/CPP and GGBFS/EPA/CPP) and unprotected (FA and GGBFS), exposed to elevated temperatures. Based on the fracture pattern observed at the point when the specimen failed, failure pattern comparisons are made. After being exposed to heating for 30 min, line crack failure was observed for the FA, FA/EPA/CPP, GGBFS, and GGBFS/EPA/CPP specimens. The specimens split into two sections along the line crack, indicating an apparent and sudden brittle failure followed by the formation of the first crack. It was observed that the line crack width was smaller in the case of the FA/EPA/CPP 30M specimens compared to the FA 30M specimens. However, the line crack width at failure in the FA/EPA/CPP 30M specimens was similar to that of the GGBFS 30M specimens. On the other hand, unprotected (FA 30M and GGBFS 30M) specimens showed surface microcracks that formed due to direct exposure to heat flux. The failure pattern observed in this case was similar to the brittle failure observed in plain cylindrical specimens under impact loadings at ambient conditions.

The failure crack patterns display significant variations as the exposure temperature exceeds 30 min. At 60 min of heating, the role of CPP protection is significantly noticeable. Critical surface microcracks were observed on the unprotected (FA 60M and GGBFS 60M) specimens. The ultimate failure resulted from the formation of multi-line cracks that developed from the fracture zone, and finally, the specimen broke into three or more pieces. In contrast, thermal microcracks were absent on the surface of both the protected (FA/EPA/CPP 60M and GGBFS/EPA/CPP 60M) specimens. Even after the initial crack appeared, these specimens continued to withstand impact loads and absorb impact energy for additional blows. The final failure pattern was curved, with zig-zag rupture failures occurring over the SCC's weakest region due to prolonged exposure to heat.

At 90 min exposure, the unprotected specimens (FA 90M and GGBFS 90M) exhibited a combination of cracking and failure. The failure pattern on the FA 90M specimen was characterised by a combination of curves and severe surface cracks that emerged from the fracture zone, resulting in a multi-curve cracking failure. Meanwhile, the GGBFS 90M heat-exposed specimens failed due to a combination of curve and line cracks and typical surface cracks seen in unprotected specimens. In contrast, the FA/EPA/CPP 90M specimens resisted developing various crack patterns. They failed through curve crack failure, similar to the failure mode observed in FA 60M specimens. The efficacy of the CPP layer was evident from the failure patterns, even after 90 min of heating. Finally, the GGBFS/EPA/CPP 90M specimens failed under multiple lines of cracks impeding the fracture zone.

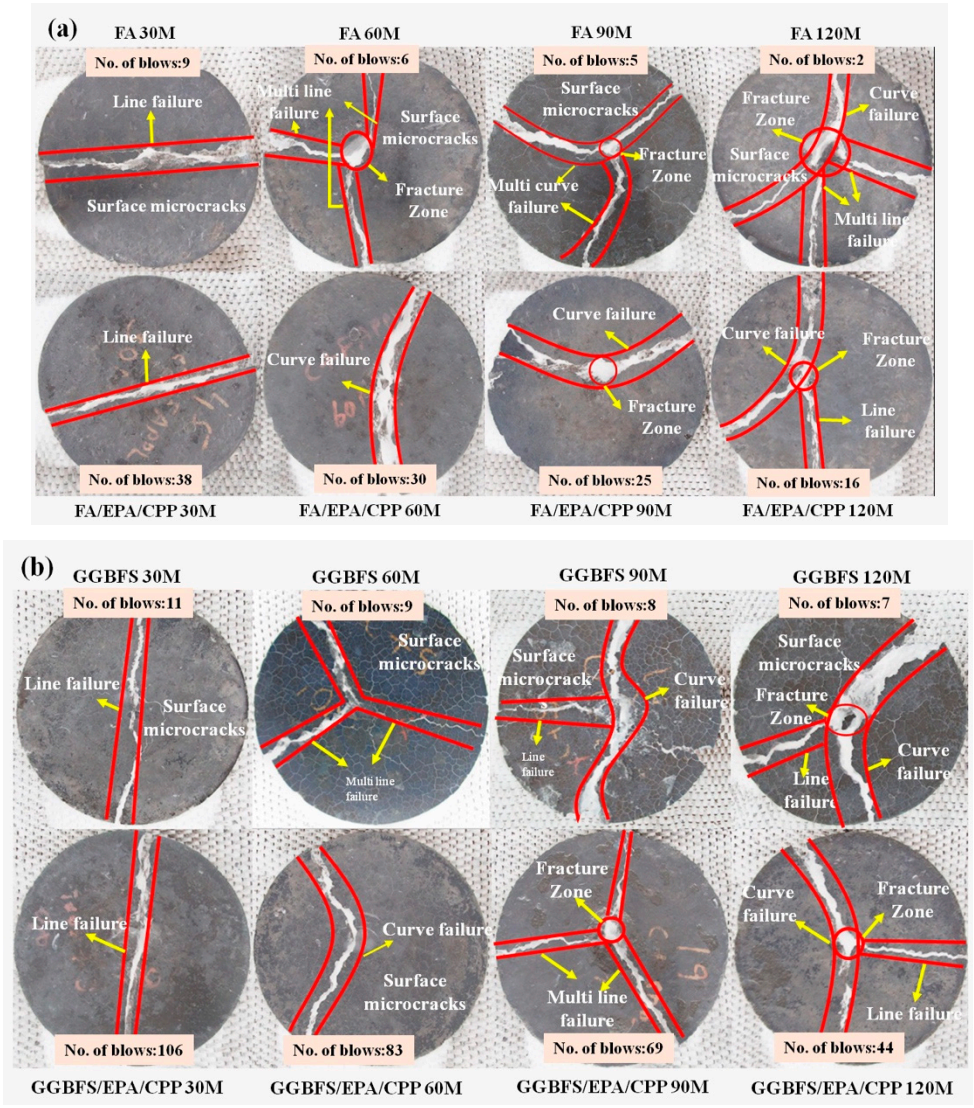


**Figure 9.** (**a**) Failure pattern of heat-exposed FA and FA/EPA/CPP specimens. (**b**) Failure pattern of heat-exposed GGBFS and GGBFS/EPA/CPP specimens.

The most significant failure pattern was observed in unprotected specimens (FA 120M and GGBFS 120M) and protected specimens (FA/EPA/CPP 120M and GGBFS/EPA/CPP 120M) after 120 min of heating. The ultimate failure observed in these specimens resembled that of the unprotected specimens subjected to a 90 min heat exposure. It was noted that irrespective of specimen protection, the ultimate failure resulted from a combination of line and curve cracks originating from the fracture zone. This indicates that prolonged high-temperature exposure diminished the effectiveness of the CPP layer. This trend is further supported by the final impact energy values obtained from the specimens heated for 120 min.

## 4. Conclusions

The detailed experimental investigation led to the following conclusions:

(i) By incorporating polycarboxylate ether-based SP, it is possible to develop SCC blends using FA and GGBFS with reduced cement content. This mixture allows for attaining the minimum quantity necessary for SCC production.

(ii) The SCC mix based on GGBFS demonstrated superior compressive strength compared to the mixtures incorporating FA and EPA. Additionally, the strength characteristics

of SCC notably improved with curing time, and the GGBFS-based SCC mix displayed greater early-age strength development compared to the FA-based SCC mix.

(iii) After the exposure durations of 60, 90, and 120 min, the failure impact energy and the number of blows exhibited a significant decline in all the reference specimens. Nevertheless, the protected specimens showed limited energy loss under the same temperature conditions. The coating layer served as a sacrifice element, improving the impact specimens' ability to withstand fire.

(iv) The decrease in strength reduction in all specimens except the CPP-coated specimens suggests that CPP coating effectively prevents strength loss at higher temperatures.

**Author Contributions:** M.E.M., T.K., A.N., A.D.A. and U.J.A.: Methodology, Formal analysis, Writing—original draft. M.E.M., T.K., A.N., A.D.A. and U.J.A.: Experimental investigation. M.E.M., T.K., A.N., A.D.A. and U.J.A.: Review and Editing. All authors have read and agreed to the published version of the manuscript.

**Funding:** This research received no external funding.

**Conflicts of Interest:** The authors declare no conflict of interest.

## References

1. Kanagaraj, B.; Kiran, T.; Anand, N.; Al Jabri, K.; Justin, S. Development and Strength Assessment of Eco-Friendly Geopolymer Concrete Made with Natural and Recycled Aggregates. *Constr. Innov.* **2022**, *23*, 524–545. [CrossRef]
2. Kanagaraj, B.; Anand, N.; Kiran, T.; Arulraj, P.; Justin, S. Experimental investigation on fresh and hardened properties of geopolymer concrete blended with recycled concrete aggregate. *Ind. Concr. J.* **2022**, *96*, 29–41.
3. Mathews, M.E.; Anand, N.; Kodur, V.K.R.; Arulraj, P. The Bond Strength of Self-Compacting Concrete Exposed to Elevated Temperature. *Proc. Inst. Civ. Eng. Struct. Build.* **2021**, *174*, 804–821. [CrossRef]
4. Neville, A.M.; Brooks, J.J. *Concrete Technology*, 2nd ed.; Pearson Education Ltd.: Harlow, UK, 2010.
5. Khoury, G.A. Passive Fire Protection of Concrete Structures. *Proc. Inst. Civ. Eng. Struct. Build.* **2008**, *161*, 135–145. [CrossRef]
6. Khoury, G.A. Concrete Spalling Assessment Methodologies and Polypropylene Fibre Toxicity Analysis in Tunnel Fires. *Struct. Concr.* **2008**, *9*, 11–18. [CrossRef]
7. Okamura, H.; Ouchi, M. Self Compacting Concrete—Research Paper. *J. Adv. Concr. Technol.* **2003**, *1*, 5–15. [CrossRef]
8. Ealiyas Mathews, M.; Anand, N.; Prince Arulraj, G.; Kiran, T. Rheological and Mechanical Characterization of Self-Compacting Concrete with Utilization of Supplementary Sustainable Cementitious Materials. *IOP Conf. Ser. Earth Environ. Sci.* **2020**, *491*, 012037. [CrossRef]
9. Sahoo, S.; Selvaraju, A.K.; Suriya Prakash, S. Mechanical Characterization of Structural Lightweight Aggregate Concrete Made with Sintered Fly Ash Aggregates and Synthetic Fibres. *Cem. Concr. Compos.* **2020**, *113*, 103712. [CrossRef]
10. Karatas, M.; Dener, M.; Benli, A.; Mohabbi, M. High Temperature Effect on the Mechanical Behavior of Steel Fiber Reinforced Self-Compacting Concrete Containing Ground Pumice Powder. *Struct. Concr.* **2019**, *20*, 1734–1749. [CrossRef]
11. Ren, J.; Wang, X.; Xu, S.; Fang, Y.; Liu, W.; Luo, Q.; Han, N.; Xing, F. Effect of Polycarboxylate Superplasticisers on the Fresh Properties of Cementitious Materials Mixed with Seawater. *Constr. Build. Mater.* **2021**, *289*, 123143. [CrossRef]
12. Nepomuceno, M.C.S.; Pereira-de-Oliveira, L.A.; Pereira, S.F. Mix Design of Structural Lightweight Self-Compacting Concrete Incorporating Coarse Lightweight Expanded Clay Aggregates. *Constr. Build. Mater.* **2018**, *166*, 373–385. [CrossRef]
13. Andrushia, D.; Anand, N.; Arulraj, P. Anisotropic Diffusion Based Denoising on Concrete Images and Surface Crack Segmentation. *Int. J. Struct. Integr.* **2020**, *11*, 395–409. [CrossRef]
14. Aslani, F.; Hamidi, F.; Ma, Q. Fire Performance of Heavyweight Self-Compacting Concrete and Heavyweight High Strength Concrete. *Materials* **2019**, *12*, 822. [CrossRef] [PubMed]
15. Kodur, V.K.R.; Harmathy, T.Z. Properties of Building Materials. In *SFPE Handbook of Fire Protection Engineering*, 5th ed.; Springer: Berlin/Heidelberg, Germany, 2016; pp. 277–324. ISBN 9781493925650.
16. Kodur, V.K.R.; Dwaikat, M. A Numerical Model for Predicting the Fire Resistance of Reinforced Concrete Beams. *Cem. Concr. Compos.* **2008**, *30*, 431–443. [CrossRef]
17. Zhai, C.; Chen, L.; Xiang, H.; Fang, Q. Experimental and Numerical Investigation into RC Beams Subjected to Blast after Exposure to Fire. *Int. J. Impact Eng.* **2016**, *97*, 29–45. [CrossRef]
18. Zhou, X.; Zhang, J. A Theoretical Study of the Effect of Coatings on Concrete Members under Fire. *Mag. Concr. Res.* **2003**, *55*, 143–149. [CrossRef]
19. Shah, S.P.; Daniel, J.I.; Ahmad, S.H.; Arockiasamy, M.; Balaguru, P.N.; Ball, C.G.; Ball, H.P.; Batson, G.B.; Bentur, A.; Craig, R.J.; et al. Measurement of Properties of Fiber Reinforced Concrete. *ACI Mater. J.* **1988**, *85*, 583–593. [CrossRef]
20. Abid, S.R.; Abbass, A.A.; Murali, G.; Al-Sarray, M.L.J.; Nader, I.A.; Ali, S.H. Post-High-Temperature Exposure Repeated Impact Response of Steel-Fiber-Reinforced Concrete. *Buildings* **2022**, *12*, 1364. [CrossRef]

21. Al-ameri, R.A.; Abid, S.R.; Murali, G.; Ali, S.H.; Özakça, M. Residual Repeated Impact Strength of Concrete Exposed to Elevated Temperatures. *Crystals* **2021**, *11*, 941. [CrossRef]
22. Mezzal, S.K.; Al-Azzawi, Z.; Najim, K.B. Effect of Discarded Steel Fibers on Impact Resistance, Flexural Toughness and Fracture Energy of High-Strength Self-Compacting Concrete Exposed to Elevated Temperatures. *Fire Saf. J.* **2021**, *121*, 103271. [CrossRef]
23. Khaliq, W.; Kodur, V. Thermal and Mechanical Properties of Fiber Reinforced High Performance Self-Consolidating Concrete at Elevated Temperatures. *Cem. Concr. Res.* **2011**, *41*, 1112–1122. [CrossRef]
24. Ríos, J.D.; Cifuentes, H.; Leiva, C.; García, C.; Alba, M.D. Behavior of High-Strength Polypropylene Fiber-Reinforced Self-Compacting Concrete Exposed to High Temperatures. *J. Mater. Civ. Eng.* **2018**, *30*, 04018271. [CrossRef]
25. Aslani, F.; Samali, B. High Strength Polypropylene Fibre Reinforcement Concrete at High Temperature. *Fire Technol.* **2014**, *50*, 1229–1247. [CrossRef]
26. Eidan, J.; Rasoolan, I.; Rezaeian, A.; Poorveis, D. Residual Mechanical Properties of Polypropylene Fiber-Reinforced Concrete after Heating. *Constr. Build. Mater.* **2019**, *198*, 195–206. [CrossRef]
27. Diana Andrushia, A.; Anand, N.; Prince Arulraj, G. A Novel Approach for Thermal Crack Detection and Quantification in Structural Concrete Using Ripplet Transform. *Struct. Control Health Monit.* **2020**, *27*, e2621. [CrossRef]
28. *IS 12269*; Ordinary Portland Cement, 53 Grade—Specification. Bureau of Indian Standards: New Delhi, India, 2013.
29. *IS 383*; Specification for Coarse and Fine Aggregates From Natural Sources for Concrete. Bureau of Indian Standards: New Delhi, India, 1970.
30. *IS 516:2014*; Method of Tests for Strength of Concrete. Bureau of Indian Standards: New Delhi, India, 2004.
31. *ACI 544.2R-89: Measurement of Properties of Fiber Reinforced Concrete (Reapproved 1999)*; ACI: Farmington Hills, MI, USA, 1999; Volume 89, p. 12.
32. Ealiyas Mathews, M.; Kiran, T.; Anand, N.; Lubloy, E.; Naser, M.Z.; Prince Arulraj, G. Effect of Protective Coating on Axial Resistance and Residual Capacity of Self-Compacting Concrete Columns Exposed to Standard Fire. *Eng. Struct.* **2022**, *264*, 114444. [CrossRef]
33. Kiran, T.; Yadav, S.K.; Anand, N.; Mathews, M.E.; Andrushia, D.; Lubloy, E.; Kodur, V. Performance Evaluation of Lightweight Insulating Plaster for Enhancing the Fire Endurance of High Strength Structural Concrete. *J. Build. Eng.* **2022**, *57*, 104902. [CrossRef]
34. Mathews, M.E.; Anand, N.; Andrushia, A.D.; Kiran, T. Investigation on Crack Control and Crack Pattern Analysis of Self-Compacting Concrete Exposed to Standard Fire Exposure. In *RILEM Bookseries*; Springer: Berlin/Heidelberg, Germany, 2021; Volume 31, pp. 127–139.
35. Yermak, N.; Pliya, P.; Beaucour, A.L.; Simon, A.; Noumowé, A. Influence of Steel and/or Polypropylene Fibres on the Behaviour of Concrete at High Temperature: Spalling, Transfer and Mechanical Properties. *Constr. Build. Mater.* **2017**, *132*, 240–250. [CrossRef]
36. Demirel, B.; Keleştemur, O. Effect of Elevated Temperature on the Mechanical Properties of Concrete Produced with Finely Ground Pumice and Silica Fume. *Fire Saf. J.* **2010**, *45*, 385–391. [CrossRef]
37. Ahmad, S.; Bhargava, P.; Chourasia, A. Direct Shear Failure in Concrete Joints Exposed to Elevated Temperatures. *Structures* **2020**, *27*, 1851–1859. [CrossRef]
38. Ganeshan, M.; Venkataraman, S. Durability and Microstructural Studies on Fly Ash Blended Self-Compacting Geopolymer Concrete. *Eur. J. Environ. Civ. Eng.* **2021**, *25*, 2074–2088. [CrossRef]
39. Kiran, T.; Anand, N.; Andrushia, A.D.; Kodur, V.; Mathews, M.E.; Arulraj, G.P. Performance of Clay Masonry Prisms with Light Weight Plaster Exposed to Standard Fire Exposure. *Fire Mater.* **2023**, *47*, 99–119. [CrossRef]
40. Kiran, T.; Anand, N.; Mathews, M.E.; Kanagaraj, B.; Andrushia, A.D.; Lubloy, E.; Jayakumar, G. Investigation on Improving the Residual Mechanical Properties of Reinforcement Steel and Bond Strength of Concrete Exposed to Elevated Temperature. *Case Stud. Constr. Mater.* **2022**, *16*, e01128. [CrossRef]